Polypyrrole-$CoFe_2O_4$ Nanocomposites: Polymer Influence on Magnetic Behavior and Particle Effects on Polymer Conduction

Ignacio Muñoz Resta, José M. Sellés, Matías Lanús-Méndez-Elizalde, Paula S. Antonel, Fernando V. Molina

Instituto de Química Física de Materiales, Ambiente y Energía (INQUIMAE), Facultad de Ciencias Exactas y Naturales, Universidad de Buenos Aires, Ciudad Universitaria, Pabellon II, piso 1, Buenos Aires C1428EGA, Argentina

Composites of cobalt ferrite nanoparticles in a polypyrrole (PPy) matrix have been synthesized in acid media and characterized by X-ray diffraction studies, scanning and transmission electron microscopy observation, thermogravimetric analysis, conductivity, and infrared spectroscopy measurements. Two types of composites were prepared: one including dodecylbenzenesulphonic acid as a particle protector and another one without protection. The magnetic behavior was studied through DC magnetization measurements; hysteresis loops were observed, showing ferromagnetic behavior for particles and composites. Materials with particle protection showed magnetic parameters independent of the PPy/ferrite ratio; in the absence of protector, both the coercivity and remanence ratio decreased as the PPy/ferrite ratio increased. These results are attributed to conducting polymer effects on the ferrite particles, affecting the magnetic anisotropy. On the other hand, composites with low PPy/ferrite ratio showed positive magnetoresistance of up to 20% at room temperature, indicating an effect of the magnetic particles on polymer conduction. POLYM. COMPOS., 00:000–000, 2017.

INTRODUCTION

In recent years, there has been a growing interest in composites formed by conducting polymers and magnetic nanoparticles (MNPs) [1–3]. Conducting polymers are very well known due to their interesting chemical, mechanical, and optical properties leading to a high number of proposed applications [4–8]. Polypyrrole (PPy) is one of the most studied among conducting polymers. It is readily synthesized by either chemical or electrochemical methods [9–11], and has been proposed for many different applications [12–14], including composites [15, 16]. MNPs are highly interesting materials, due to their potential applications in different fields [17–19]. Whereas larger particles are composed of several magnetic domains, below a certain (composition dependent) critical size, MNPs behave as monodomains, which give rise to interesting properties [1, 17, 20]. Several materials have been investigated, mainly iron and iron oxides [21, 22], ferrites [23, 24], and other metals [25, 26]; among these, cobalt ferrite ($CoFe_2O_4$) is highly interesting as it is a hard material from the magnetic point of view (exhibiting ferromagnetism at room temperature), has a high coercive field and moderate saturation magnetization and, in addition, displays excellent chemical stability [27].

A number of magnetic nanoparticle-conducting polymer composites have been proposed, mainly based on polypyrrole [28–31], poly(ethylenedioxitiophene) [32, 33], and poly(aniline) (PANI) [34, 35]. The use of conducting polymers gives rise to materials with properties that would be difficult to obtain with the individual components, as they have both high magnetic susceptibilities and high conductivity [36, 37]. These magnetic composite materials comprise a new generation of multifunctional materials that combine the properties of ordinary polymer and magnetic materials (ferri- and/or ferromagnetic particles mixed or embedded in a matrix). Such materials have been proposed for several applications: Radhakrishnan et al. [38] synthesized PANI–Fe_3O_4 composites and showed its application as an electrochemical dopamine sensor and supercapacitor material; Bhaumik et al. [39] demonstrated the use of PPy–magnetite composites for fluoride adsorption and removal from water; Wuang et al. [40] obtained PPy–Fe_3O_4 nanoparticles functionalized with folic acid for cancer treatment; many studies have been devoted to the application for microwave shielding [41, 42]. All these applications underline the importance of the study of these materials from an applied point of view, besides the fundamental interest.

Correspondence to: F. V. Molina; e-mail: fmolina@qi.fcen.uba.ar
Contract grant sponsor: Universidad de Buenos Aires; contract grant numbers: 20020130100035BA, 20020120300007BA; contract grant sponsor: Agencia Nacional de Promoción Científica y Tecnológica; contract grant numbers: PICT 2014 N° 2289, PICT 2014 N° 1194.
DOI 10.1002/pc.24575
Published online in Wiley Online Library (wileyonlinelibrary.com).

In this work, $CoFe_2O_4$–PPy composites have been prepared by a wet chemical method, with *in situ* pyrrole polymerization. The synthesis was performed both in the absence and in the presence of dodecylbenzenesulfonic acid (DBSA) as a particle-protecting agent. The composites were characterized by XRD studies, SEM and TEM observation, thermogravimetric analysis, conductivity measurements, IR spectroscopy, DC magnetization, and magnetoresistance measurements.

MATERIALS AND METHODS

AR grade chemicals, supplied by Sigma-Aldrich, and high purity water from a Milli-Q system were employed throughout. Pyrrole (Py) was used as received.

Synthesis of Cobalt Ferrite Nanoparticles

The synthesis of $CoFe_2O_4$ nanoparticles was performed following Antonel et al. [3]. Briefly, 22.25 mL of a solution containing 0.450 M $FeCl_3{\cdot}6H_2O$ and 0.225 M $CoCl_2{\cdot}6H_2O$ (2:1 Fe(III)–Co(II) molar ratio), in 0.4 M HCl, was added dropwise to 200 mL of 1.5 M NaOH, keeping the pH adjusted at 12, under constant high speed stirring. The synthesis temperature was set at 80°C, using a water-jacketed reaction vessel with a circulating thermostatic bath. Dark brown $CoFe_2O_4$ nanoparticles precipitated immediately after the first drops of the Fe(III)–Co(II) solution. The temperature of synthesis and the high speed stirring were kept constant during the addition of the cationic solution. After the addition of this solution, the reaction media was maintained at 80°C, at high speed stirring, for 2 h. The $CoFe_2O_4$ nanoparticles were separated by centrifugation at 12,000*g* during 20 min at room temperature. The pellet was washed with Milli-Q water, repeating the cycles of washing–centrifugation until neutral pH of the supernatant was reached (about 10 times). Finally, the $CoFe_2O_4$ nanoparticles were dried using a vacuum oven at 40°C during 24 h.

Synthesis of $CoFe_2O_4$–PPy Composites

Two series of $CoFe_2O_4$–PPy composites were synthesized: one with the inclusion of DBSA as a protecting agent of the MNPs, and the second one without DBSA. The synthesis was performed following Muñoz Resta et al. [33] with some modifications. For the composites without DBSA, 100 mg of $CoFe_2O_4$ nanoparticles were added to 50 mL of MilliQ water. This mixture was subjected to ultrasound treatment and vigorous mechanical stirring for 30 min, to disperse the NP. Then, *p*-toluensulfonic acid (*p*-TSA) and Py monomer (in a given molar ratio, r_{Py}, with respect to ferrite, see below) were added, in a molar ratio 1:1, keeping the mixture for 1 h in the same conditions. Finally, ammonium persulfate (APS), in a ratio 1:1 with respect to Py, was added. After that, the mixture was maintained for 1.5 h always under ultrasound treatment and mechanical stirring. For the synthesis with DBSA, the procedure was slightly different. In this case, 100 mg of $CoFe_2O_4$ nanoparticles were added to 50 mL of a 0.1 M DBSA solution and a combined treatment of ultrasound and strong mechanical stirring was applied throughout the whole procedure to efficiently disperse the NP. It was first maintained during 30 min to allow DBSA adsorption onto the particles. Then, Py monomer (in a giver molar ratio, r_{Py}, with respect to ferrite, see below) was added keeping the reaction mixture for 1 h in the same conditions. Finally, APS in a molar ration 1:1 with respect to Py was added. After APS addition, the reaction mixture was kept for 1.5 h. After that, the agitation was removed and the product was demulsified with an equal volume of isopropyl alcohol. For both procedures (without and with DBSA) the black precipitates was separated by centrifugation at 15,000*g* and 17°C for 10 min. The pellet was repeatedly washed with MilliQ water and ethanol, to remove the excess of reactants and oligomers (by-products of the polymerization reaction). Finally the composites were dried at room temperature for 24 h

The synthesis was performed for different values of the molar ratio in the feed:

$$r_{Py} = \frac{n_{Py}}{n_{CoFe_2O_4}} \tag{1}$$

where n_{Py} and $n_{CoFe_2O_4}$ are the mole numbers of pyrrole monomer and $CoFe_2O_4$, respectively. In the above specified conditions, r_{Py} was varied between 0.5 and 10.

Characterization of $CoFe_2O_4$ Nanoparticles and $CoFe_2O_4$–PPy Composites

X-Ray Diffraction (XRD). X-ray powder diffraction analysis of the nanoparticles was performed with a Philips X-Pert diffractometer using Cu K_α radiation ($\lambda = 0.154056$ nm); the average crystallite size was determined with the Scherrer equation:

$$d_C = \frac{A\lambda}{\beta \cos\theta} \tag{2}$$

where A is the shape factor, taken here as 0.9, β is the full width at half maximum of the peak, and θ is the corresponding Bragg angle.

Electron Microscopy Studies. The particle size, morphology, and composition of particles and composites were studied by transmission electron microscopy (TEM), scanning electron microscopy (SEM), energy-dispersive X-ray spectroscopy (EDS), and backscattered electron detection. TEM observation was done with a Philips EM 301 microscope. Each material (nanoparticles or composites) was suspended in acetone and approximately 10 μL of suspension were dripped on a TEM grid and dried prior to insertion in the TEM column. SEM analysis was performed using a

 DOI 10.1002/pc

Zeiss Supra 40 Gemini microscope, equipped with an EDS detector, and a four-quadrant solid-state detector (QBSD, Oxford Instruments), which collects backscattered electron scattered under very low angle. The samples were prepared by placing a small amount of each solid (nanoparticles or composites) in one side of a carbon tape. EDS and QBSD measurements were performed in the same experiment.

Thermal Analysis. Thermogravimetric analysis (TGA) of $CoFe_2O_4$ nanoparticles, $CoFe_2O_4$–PPy composites, and pure PPy polymer was performed using a thermobalance TG-DTA 50 simultaneous Shimadzu. The TGA thermograms were recorded for 10–20 mg of each sample at a heating rate of 10°C/min in the temperature range of 25–800°C under air atmosphere.

Fourier Transform Infrared Spectroscopy (FTIR). The infrared (IR) measurements of composites, nanoparticles, and polymer were performed using an FTIR Nicolet 8,700 spectrometer, in the range 400–4,000 cm^{-1}. The samples were pressed into pellets prepared dispersing 0.5 mg of each one in 150 mg of KBr. For each sample, 32 scans were accumulated.

Conductivity Measurements. The conductivity of the different samples was measured on pressed circular pellets (1 cm diameter) using a Teq-03 (S. Sobral, Buenos Aires, Argentina) potentiostat under computer control. Following Ohm's law, a known current was applied and the potential difference was measured and averaged during 120 s. The pellet thickness was measured with a caliper to compute the conductivity.

Magnetization and Magnetoresistance Studies. A Lakeshore 7,400 vibrating sample magnetometer (VSM) was used for recording magnetization curves at room temperature. The samples were prepared by packing with Teflon tape 10–20 mg of each composite. The resistance of the different samples was also measured in the presence of an applied magnetic field, between 0 and 4,500 G, using the same VSM. Percent magnetoresistance (*MR%*) was calculated following *Eq. 3*:

$$MR\% = 100\frac{R_H - R_0}{R_0} \tag{3}$$

where R_H is the resistance at the applied magnetic field, H, and R_0 is the resistance in the absence of a magnetic field.

RESULTS AND DISCUSSION

Particle Size and Composites Morphology

The morphology of the cobalt ferrite particles obtained here was very similar to those of Antonel et al. [35], prepared with the same technique. Briefly, the particle size, as verified by SEM and TEM imaging with the aid of the ImageJ software, was found to be $d_P = (17.3 \pm 1.0)$ nm, being within the range of monodomain magnetic particles, which for cobalt ferrite falls between a minimum of 7–9 nm [23, 43] and a maximum of about 60–70 nm [44, 45].

The morphology of some of the obtained composites is observed in Fig. 1a–h, as revealed by SEM observation; Fig. 1i shows the SEM image of pure PPy for comparison.

Figure 2 presents the examples of TEM images of composites, showing the cobalt ferrite particles embedded in the polymer. The darker areas correspond to thicker parts of the composite material.

Different morphologies are found for low and high values of r_{Py}. Composites with low polymer content have a relatively smooth topography, as a consequence of being dominated by the nanoparticles (Figs. 1a–c and 2a); through QBSD it is possible to confirm that composite with $r_{Py} = 0.5$ is composed by a high proportion of $CoFe_2O_4$ nanoparticles (bright areas with QBSD detector, Fig. 1c). On the other hand, for high polymer content, the materials show a more irregular surface, with a globular-like structure, very similar to the pure polymer; as the particles content increases, the polymer growth is affected by their presence, resulting in morphology changes as observed [35]. Besides, the presence of PPy favors the dispersion of the nanoparticles (Fig. 1d–g and 2b and c), as they appear more separated with the increase in r_{Py}. The presence of DBSA does not cause, at least in the TEM/SEM observation, significant changes to composite morphology.

Crystalline Structure

The XRD patterns of the particles obtained are shown in Fig. 3, where a typical inverse spinel pattern is observed (ICDD 03–0864), very similar to that of Fe_3O_4 [23, 46]. The diameter of the crystallites, d_c, prepared here was estimated through *Eq. 2* using the (311) peak, resulting in $d_c = 16.5$ nm which is in agreement with reported values [3, 23] and with the microscopy results.

Figure 4 shows the XRD patterns for composites with different monomer/NMPs ratios (r_{Py}), with DBSA as protector (a, c, e) and without DBSA (b, d, f). It is clearly observed the transition from a NMPs-dominated composite (in Fig. 4a,b) to a polymer dominated material (Fig. 4e,f), characterized by a broad diffraction band around $2\theta = 20°$, characteristic of the low crystallinity of the polymer. The transition point is different for composites containing DBSA, where a mixed pattern is found about $r_{Py} = 3.5$, than in absence of the surfactant, with the mixed pattern resulting near $r_{Py} = 5.0$. By comparing Fig. 4d,e ($r_{Py} = 5$), it is clear that the synthesis with DBSA gives a material that is essentially PPy (e), while without DBSA the $CoFe_2O_4$ pattern is still observed. This result suggests that in the presence of DBSA the polymerization yield is enhanced. Also, these results are consistent with the SEM observations, which show particle-dominated composites for $r_{Py} \leq 2$ and polymer-dominated materials

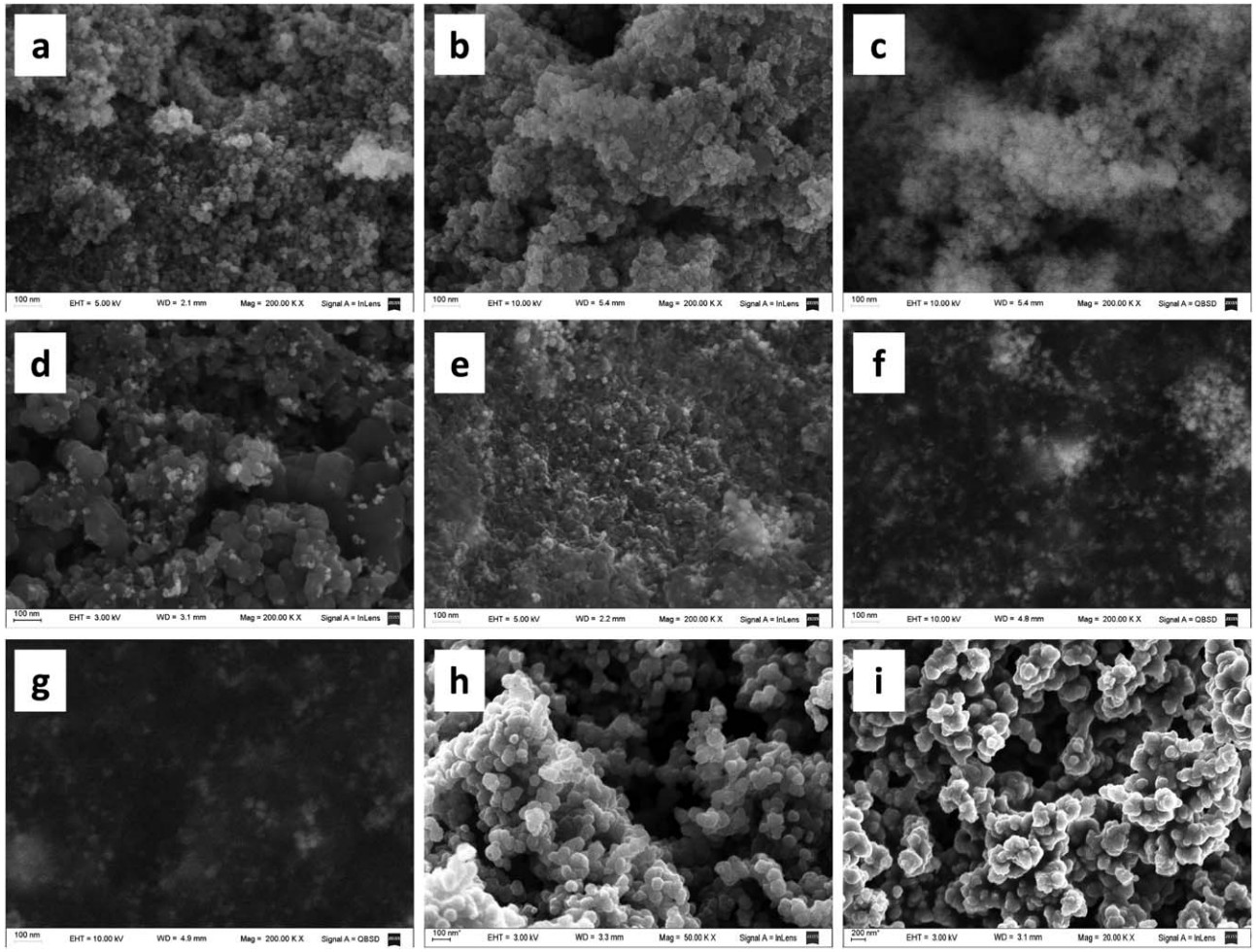

FIG. 1. SEM images of $CoFe_2O_4$–PPy composites: (a) without DBSA, $r_{Py} = 0.5$; (b) with DBSA, $r_{Py} = 0.5$; (c) same as (b) with QBSD detector; (d) without DBSA, $r_{Py} = 2.0$; (e) with DBSA, $r_{Py} = 2.0$; (f) the same as (e) with QBSD detector; (g) with DBSA, $r_{Py} = 3.5$, QBSD detector; (h) without DBSA, $r_{Py} = 10.0$; (i) pure PPy.

for $r_{Py} > 5$. Particle diameter determinations from XRD patterns of composites where the inverse spinel peaks are discernible (i.e., $r_{Py} < 5$ with DBSA and $r_{Py} < 10$ in its absence) give results in the range 16–17 nm, thus no changes in particle size are observed upon composite formation. To investigate the presence of long-range order in the composites, some XRD measurements were extended to $2\theta = 2°$ (not shown), but no pattern was observed below $2\theta = 10°$, thus no evidence of the existence of particle ordering was found, in agreement with microscopy observations.

Thermal Stability and Composition

To study the thermal stability of the resulting composites and to gain insight into their composition, thermogravimetric (TG) analysis in air was conducted (Fig. 5); it is observed that PPy is completely decomposed by oxidation and the ferrite particles undergo only a small mass loss, whereas the composites give intermediate results, thus confirming the composite formation. The features in Fig. 5 can be explained as follows: first, an initial mass loss is observed, attributable to removal of water from the material; this loss ends at about 200°C, where the curves are almost leveled. At higher temperature, *T,* values a pronounced decrease is observed, corresponding to polymer decomposition, starting between $\sim$ 300°C and ending at $\sim$ 600°C. On the other hand, pure ferrite particles show, after some water elimination, a small decrease probably due to loss of surface hydroxyl groups. In the presence of DBSA, some differences are observed: first the initial mass loss is smaller, which can be attributed to the less hydrophilic character of this surfactant, and second the onset of polymer decomposition is shifted to higher temperatures for about 100°C, suggesting a thermal stabilization of PPy in the presence of DBSA. From the TG results, the composites composition can be estimated, assuming that the mass loss at $T < 220$°C is due to water elimination, that the remaining mass at $T = 800$°C corresponds to the ferrite particles with no polymer remaining, and introducing a correction for the mass change of the cobalt ferrite particles between 25 and 800°C. The results for the $CoFe_2O_4$ mass fraction in the composite, f_{CF}, and the measured polymer/ferrite molar ratio, r_m are presented

 DOI 10.1002/pc

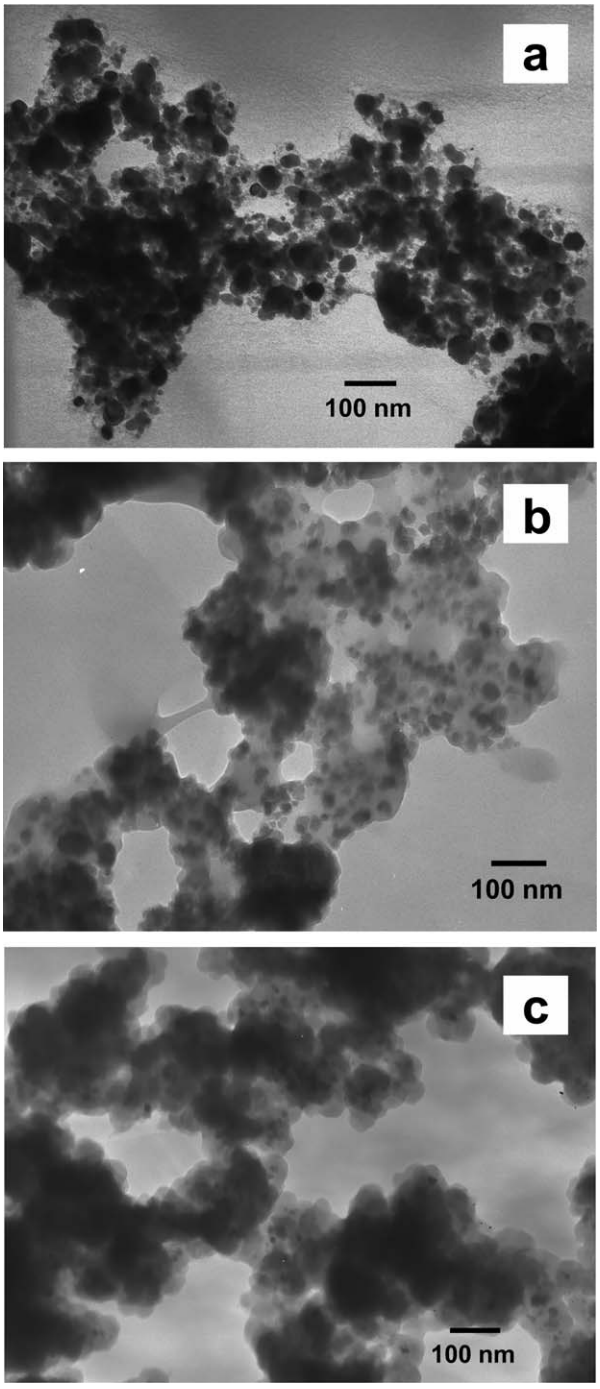

FIG. 2. TEM images of composites without DBSA for (a) $r_{Py} = 0.5$; (b) $r_{Py} = 1.0$ and (c) $r_{Py} = 5.0$.

in Table 1. In the case of DBSA protected particles, this surfactant could not be differentiated from the polymer in the thermograms, thus the r_m results given in Table 1 for these composites should be taken with caution, especially for low r_{Py} cases.

It is worth noting that in the presence of DBSA, the resulting polymer/oxide ratio is higher than in its absence, indicating higher reactivity and/or polymerization rate, consistent with XRD results; for $r_{Py} \geq 5$, the amount of particles in the composite was very low and could not be determined accurately.

Electrical Conductivity

The electrical conductivity of the composites obtained here resulted nearly independent of the monomer–ferrite ratio, being in the range 0.01–0.1 S cm^{-1}, with pure PPy prepared in the same conditions giving a conductivity of 0.16 S cm^{-1}. These values show that the presence of the MNPs does not have a strong effect on the polymer electrical conductance, suggesting that, even for low values of r_{Py}, PPy retains an electrical conductance path, that is, the polymer is able to percolate through the material.

IR Spectroscopy. IR spectroscopy gives confirmation of the presence of the diverse components and provides information about their interactions. Representative IR spectra are shown in Fig. 6. In Fig. 6a, the spectra obtained in absence of DBSA are collected: from bottom up, the spectra of $CoFe_2O_4$, of composites with increasing r_{Py}, and of pure PPy are shown. The IR response of PPy (Fig. 6a, top) has been studied by several authors [47–51]; the main bands corresponding to N—H stretching ($\sim$ 400 cm^{-1}), ring stretching and deformation (1,550, 1,460, and 1,320 cm^{-1}), C—H in-plane bending (1,100 cm^{-1}) and out-of-plane bending (1,050 cm^{-1}), ring out-of-plane vibrations (910 cm^{-1}), and C—H/N—H out-of-plane bending (790 cm^{-1}) are observed. There is a strong band at 1,180 cm^{-1} which can be assigned to N—H in-plane bending [48, 50], but in some spectra is not observed, and has been also attributed to overoxidation products [51]. In the spectrum of cobalt ferrite (bottom), on the other hand, besides surface OH vibrations $\sim$3,500 cm^{-1} and other minor bands, the main lattice band at 590 cm^{-1} is clearly visible. In the composite spectra, this band shows decreasing intensity as r_{Py} increases, as expected. There are some differences between the polymer bands in pure PPy spectrum and those in the composites: first, a weak band at

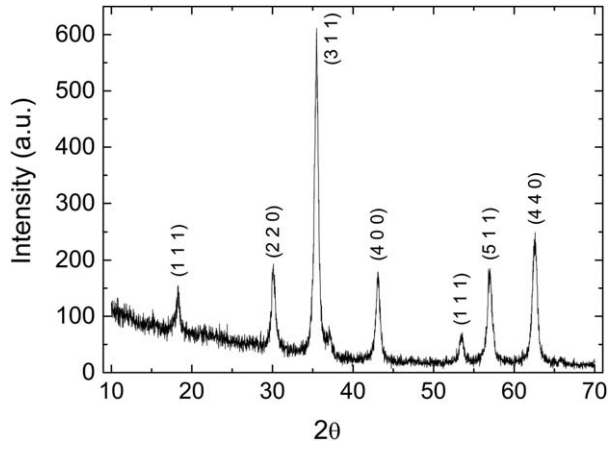

FIG. 3. XRD diagram of $CoFe_2O_4$ nanoparticles synthesized at 80°C, revealing an inverse spinel structure.

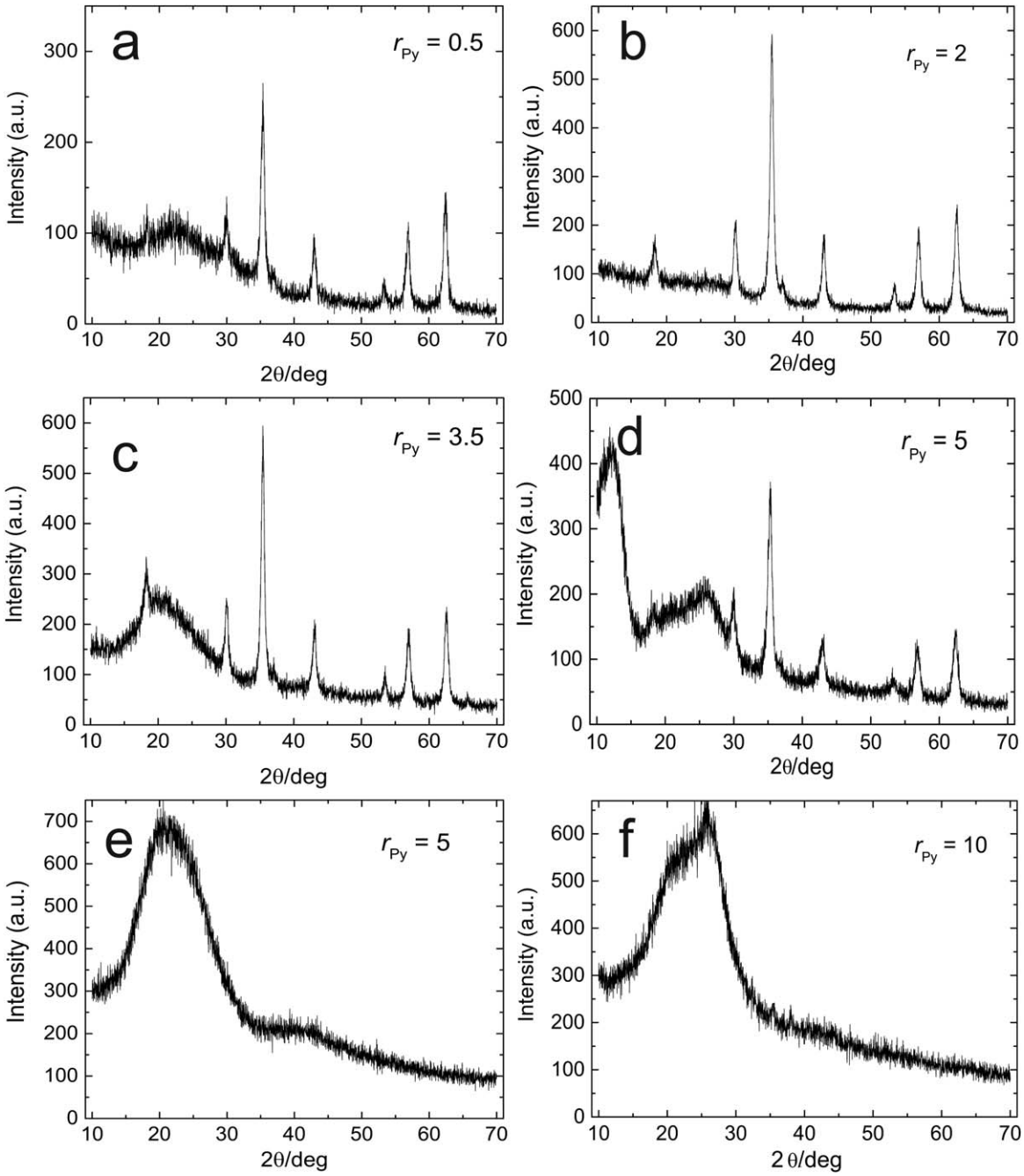

FIG. 4. XRD patterns of composites for different r_{Py} ratios with DBSA (a, c, and e) and without DBSA (b, d, and f).

1,640 cm^{-1} is discernible, which can be attributed to ring stretching modes [50]; also, displacements of ring modes are observed: 1,550–1,560 cm^{-1}, 1,320–1,330 cm^{-1}, and 910–926 cm^{-1}. All these differences are consistent with ring symmetry changes caused by polymer–particle interactions. Figure 6b shows the spectra when DBSA is included as a protective agent. The DBSA spectrum is at bottom, where the most prominent feature is the group of C—H stretching bands around 2,900–3,000 cm^{-1}; these bands are observed in all the composite spectra, and also in the spectrum of PPy synthesized in the presence of the surfactant, top. This last spectrum shows some changes compared with the pristine PPy one at the top of Fig. 6a: the ring stretching bands appear at 1,560, 1,464, and 1,300 cm^{-1}, C—H in-plane and out-of-plane bending at 1,124 and 1,036 cm^{-1} respectively, and ring out-of-plane at 920 cm^{-1}, thus indicating interactions between the particle and the surfactant. However, in the composites, there are only minor changes from these values, thus confirming that DBSA effectively isolates the particles from the polymer.

 DOI 10.1002/pc

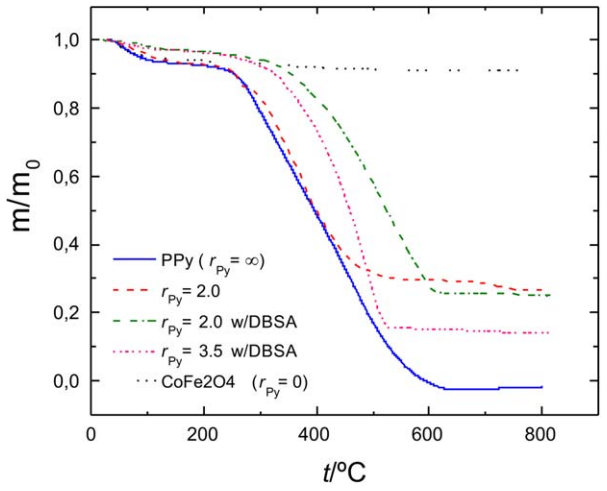

FIG. 5. TG measurements of cobalt ferrite, PPy, and composites, plotted as relative mass (m/m_0) as a function of temperature. [Color figure can be viewed at wileyonlinelibrary.com]

Magnetization Behavior

Figure 7 shows the mass magnetization, M, as a function of the magnetic field H for the bare particles and composites, both without and with DBSA. Composites with $r_{Py} > 5$ in absence of DBSA, and with $r_{Py} > 3.5$ in its presence, showed very low magnetic response, in agreement with the results of Fig. 4. The magnetization is referred to the composite mass, thus the curves have smaller M values as the contents of magnetic particles decreases; however, normalizing by the true particles mass, as reported in Table 1, leads to similar maximum values for the different curves, within experimental error. The curve for the bare particles is similar to others reported in the literature [3, 23, 43], showing hysteresis which reveals ferromagnetic behavior. The curves for the composites show a similar behavior, indicating that the particles essentially keep their ferromagnetic nature, as it has been reported for similar composites [35, 52]; at the extremes of the H range (± 1.0 T), the curve corresponding to the bare particles ($r_{Py} = 0$) reaches a value $M_{max} = 54$ emu g^{-1}, somewhat lower than the saturation magnetization reported for cobalt ferrite particles of about 70 emu g^{-1} [3, 23].

To compare more closely the above curves, they are presented in Fig. 8 in the form of relative magnetization $m = M/M_{max}$. The inset shows the curves in the full range, where it is observed that all the curves merge for high field values, showing the same slope. The main graph shows an enlarged view of the low field region, revealing that all the curves merge closely in the presence of DBSA, whereas without the surfactant differences in the coercivity, H_c, and relative remanence, m_r, are found. These values, as determined from linear fit to the rising part of the upper curve near $H = 0$, are collected in Table 2.

In the absence of protection, both H_c and m_r decrease as r_{Py} increases, whereas with protection, these values are constant within experimental error. The coercive field in the presence of DBSA is lower than for the bare particles; this change can be attributed to a decrease of particle size due to the low pH polymerization conditions. In the absence of DBSA, the noticeable decrease of H_c cannot be solely due to particle size, as the polymerization procedure is the same. A similar behavior was observed by Prasanna et al. [53] in cobalt ferrite-PANI composites. These results indicate that there is a change in the magnetic properties due to interaction with the PPy matrix when the particles are included in the composite without DBSA; otherwise, when a simple "dilution" effect is taking place all the normalized curves are coincident, as observed in Fig. 8b. Dipolar and exchange interactions are the most important forms of magnetic interactions [54], both capable of causing ferromagnetic behavior for nanoparticles which isolated would display superparamagnetic response; however, such effect would be only dependent on the interparticle distance and independent of the matrix composition, which is not the case here.

Interactions between MNPs and the conducting polymer matrix have been observed in other studies: Wu et al. [55] found a decrease in H_c with PANI contents in $Ni_{0.5}Zn_{0.5}Fe_2O_4$/polyaniline composites, attributed to polymer/particle interactions; Montoya et al. [56] observed redox interactions between matrix and particles in PPy–magnetite composites; Antonel et al. [35] observed changes in the magnetic properties (coercivity and remanence ratio) of cobalt ferrite particles in composites with PANI attributed to magnetic coupling with PANI unpaired spins; Zhang et al. [57] found increased extinction coefficients of magnetite MNPs when coated with PPy, interpreted as due to electron injection form the polymer into the oxide. The interactions leading to changes in coercivity and remanence can be related to a

TABLE 1. Composites composition as found by thermogravimetric analysis.

	No protection		With DBSA	
Feed composition, r_{Py}	Measured composition, r_m	Cobalt ferrite mass fraction, f_{CF}	Measured composition, r_m	Cobalt ferrite mass fraction, f_{CF}
0.5	0.81	0.81	2.3	0.61
1.0	2.1	0.63		
2.0	8.7	0.29	9.8	0.27
3.5			20.5	0.15
5.0	22	0.14	>300	
10.0	155	0.02	>300	

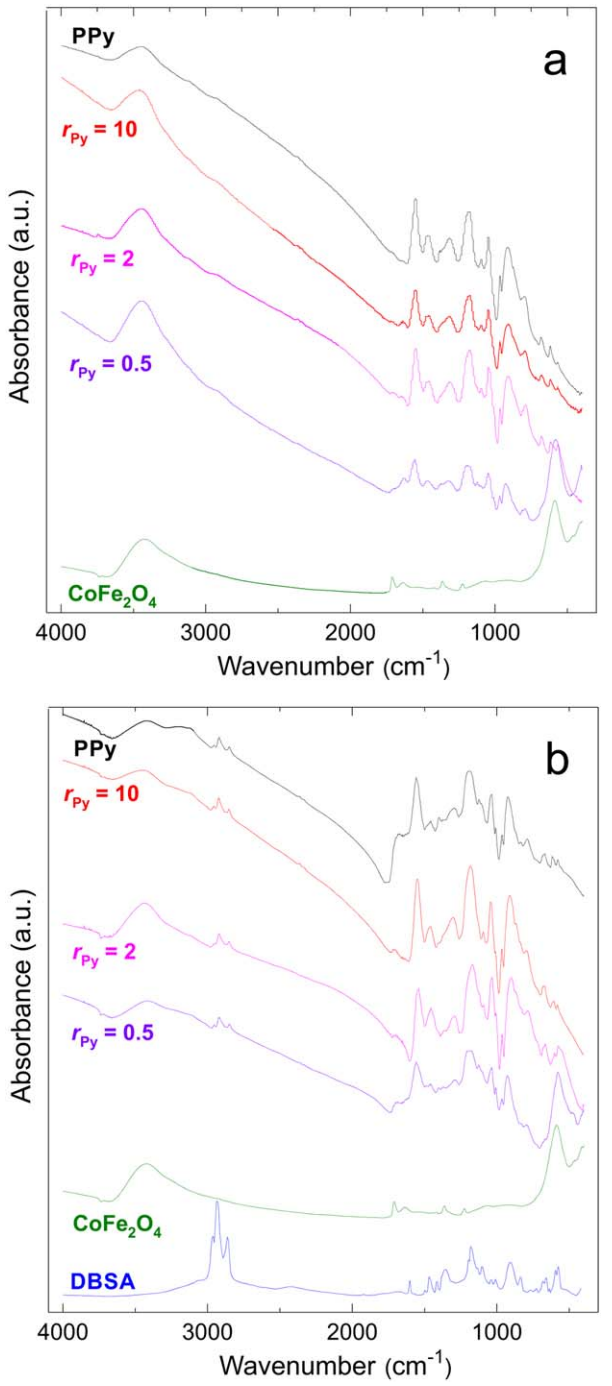

FIG. 6. IR spectra of composites (a) without DBSA and (b) with DBSA as protector. Including the $CoFe_2O_4$ spectrum and, in (b), the DBSA spectrum and that of PPy polymerized in the presence of DBSA. [Color figure can be viewed at wileyonlinelibrary.com]

modified magnetic anisotropy; for small, single-domain ferromagnetic particles, the coercivity is limited by

$$H_c \leq \frac{2K}{M_s} \tag{4}$$

where K is the net anisotropy and M_s is the saturation magnetization. According to Bødker et al. [58], the net anisotropy of a small particle has two contributions, which for a cubic or spherical particle can be written:

$$K = K_b + \frac{6}{d}K_s \tag{5}$$

where K_b and K_s are the bulk and surface anisotropies, respectively and d is the cube side. K_s is different from the bulk due to reduced symmetry and can be affected by surface interactions and processes [59]. As pointed out by several authors [33, 55, 60], interactions with the polymer matrix can decrease the surface anisotropy K_s and thus lead to a decrease in H_c; the dependence on the polymer/oxide ratio can be attributed to an increased particle coverage as this ratio increases. Furthermore, here we suggest a microscopic explanation for the observed effect: as it is already known, cobalt ferrite has a strong ferromagnetic

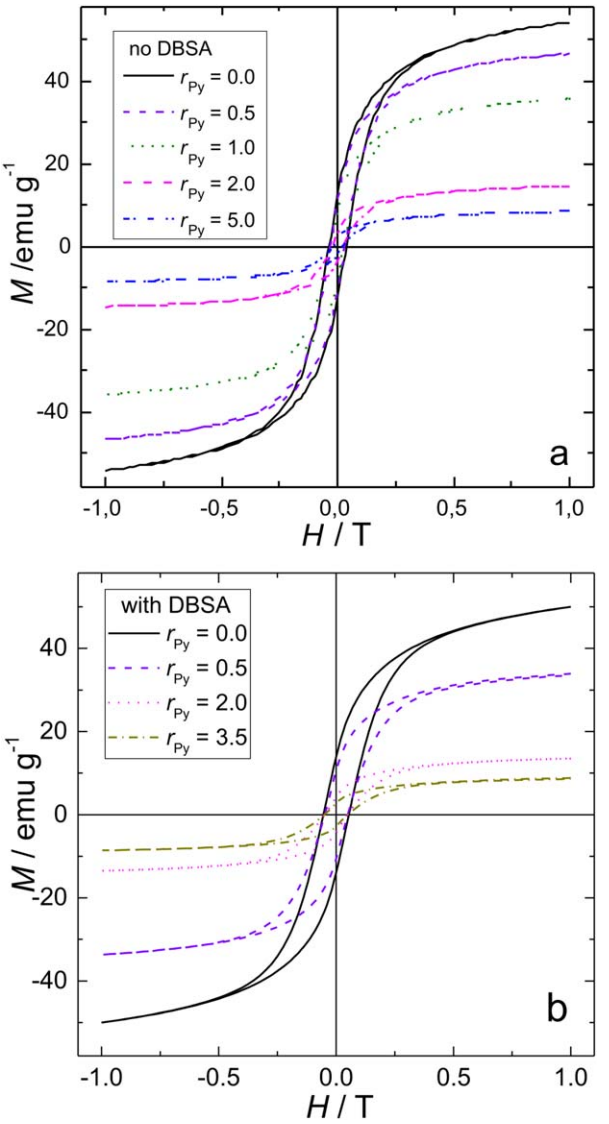

FIG. 7. Magnetization curves of $CoFe_2O_4$ particles and composites in the (a) absence and (b) presence of DBSA. [Color figure can be viewed at wileyonlinelibrary.com]

DOI 10.1002/pc

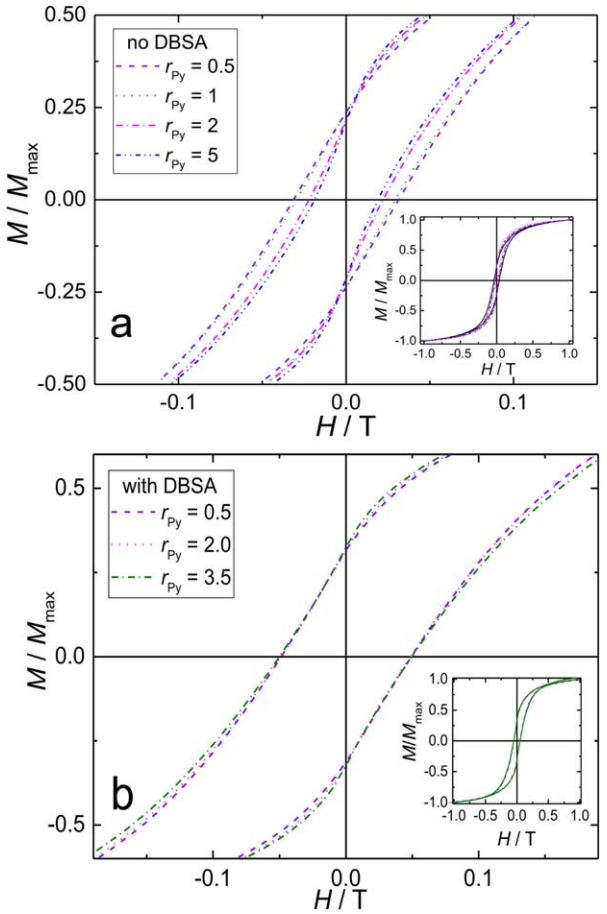

FIG. 8. Normalized magnetization curves for $CoFe_2O_4$–PPy composites, in the (a) absence and (b) presence of DBSA. The insets show the full curves, and the main graphs present an enlargement about $H = 0$. [Color figure can be viewed at wileyonlinelibrary.com]

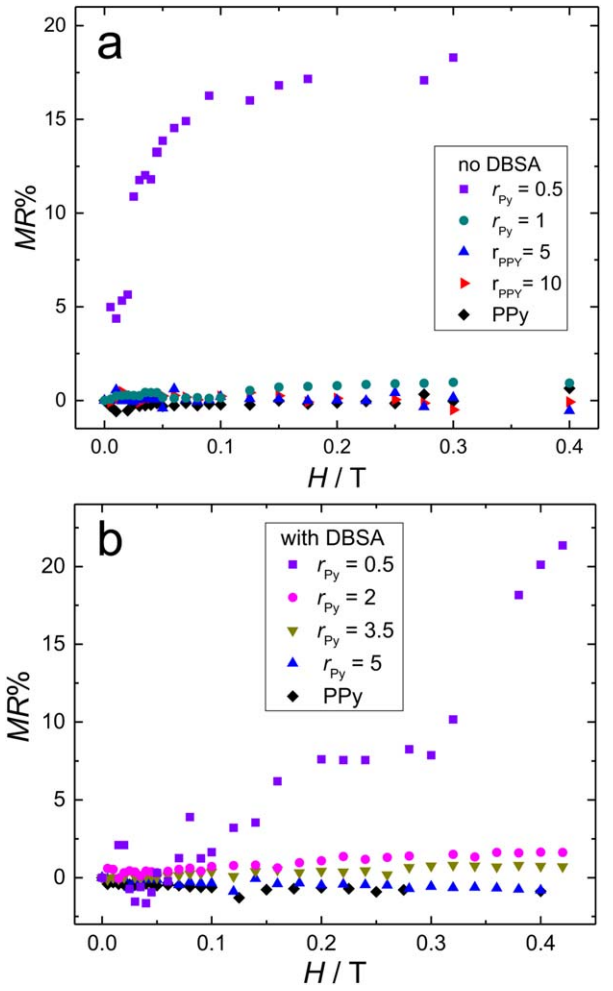

FIG. 9. Magnetoresistance for PPy and $CoFe_2O_4$–PPy composites in the (a) absence and (b) presence of DBSA at room temperature. [Color figure can be viewed at wileyonlinelibrary.com]

behavior due to the Co^{2+} ion structure, its highest occupied molecular orbital being doubly degenerate [61]; following Zhang et al. [57], the conducting polymer can inject electrons into the oxide, which in turn could occupy Co^{2+} molecular orbitals and break the degeneration, thus decreasing the particle anisotropy and the coercivity.

Magnetoresistance

Figure 9 shows the MR%, computed from *Eq. 3*, of pure PPy and $CoFe_2O_4$–PPy composites at room temperature, in the absence (a) and presence (b) of DBSA. In both cases, MR% is related to r_{Py}, being positive and increasing in value for composites with low PPy contents ($r_{Py} \leq 1$), as already seen by Gu et al. for composites of PANI–magnetite [34]. On the other hand, for pure PPy and composites with high PPy contents ($r_{Py} > 1$), MR% is negative, as already reported by Long et al. [62] and Romero et al. [63], for pure PPy and pure PANI. Also in both cases (synthesis without and with DBSA), MR% reached values up to 20% for composites with $r_{Py} = 0.5$ while for composites with $r_{Py} \geq 1$, the maximum MR% is about 1%. This difference is clearly due to the polymer-ferrite ratio: for the lowest r_{Py} value studied here, the highest magnetoresistance is observed, consistent with a close polymer-ferrite interaction; presumably, in this case, all PPy present is interacting with the particles and thus

TABLE 2. Coercive field and remanence ratio of cobalt ferrite and composites.[a]

Material	$CoFe_2O_4$	$r_{Py} = 0.5$ no DBSA	$r_{Py} = 1.0$ no DBSA	$r_{Py} = 2.0$ no DBSA	$r_{Py} = 5.0$ no DBSA	$r_{Py} = 0.5$ w/DBSA	$r_{Py} = 2.0$ w/DBSA	$r_{Py} = 3.5$ w/DBSA
H_c/Oe	542 ± 14	316 ± 33	298 ± 24	226 ± 36	199 ± 45	491 ± 28	489 ± 20	499 ± 29
m_r	0.270 ± 0.007	0.228 ± 0.009	0.230 ± 0.007	0.208 ± 0.012	0.202 ± 0.017	0.306 ± 0.007	0.309 ± 0.005	0.310 ± 0.007

[a]95% confidence intervals are reported.

affected by the magnetic field, whereas for higher r_{Py} values, only part of the polymer is interacting with the MNPs, thus electric conduction is mainly carried by the noninteracting PPy part.

At variance with the magnetic properties of the MNPs, in this case, the polymer electrical conduction is affected essentially equal in the absence and presence of DBSA. It is difficult at present to establish the nature of the interactions involved; for polyaniline–$CoFe_2O_4$ composites, changes in magnetic behavior have been attributed to coupling between the MNP magnetic moments and unpaired spins in the polymer matrix [35]; however, for PPy, this appears to be less probable. Further studies are required to elucidate this point.

An interesting feature in Fig. 9a is that the composite with $r_{Py} = 0.5$ shows a linear response with the applied magnetic field up to 0.1 T. This result suggests the potential use of this composite as an active element in electronic devices, for example, in magnetic field sensors. To the best of our knowledge, this is the first time that magnetoresistance measurements of PPy–$CoFe_2O_4$ composites are investigated.

CONCLUSIONS

The synthesis of cobalt ferrite–polypyrrole nanocomposites with and without DBSA protections revealed the polymer influence on the magnetic properties of the resulting material. Both coercivity and remanence ratio decrease as the polymer/oxide ratio increases. The effect can be attributed to polymer induced changes of the surface anisotropy of the magnetic particles. The injection of polymer conduction electrons into the oxide particles, which could affect the cobalt ions electronic structure, is suggested as a cause of the observed behavior. Magnetoresistance measurements reveal in turn the effect of the magnetic MNPs on the polymer conductivity. The composites with low r_{Py} ratio are promising for potential applications, as magnetic field sensors.

ACKNOWLEDGMENTS

The collaboration of A. G. Leyva in the thermogravimetric measurements is gratefully acknowledged. P. S. A. and F. V. M. are the members of the Carrera del Investigador Científico of CONICET. I. M. R. and J. M. S. performed equally the experimental part; M. L. M. E. performed the magnetoresistance measurements; P. S. A. devised and supervised the experiments; P. S. A. and F. V. M. analyzed the results; F. V. M. wrote the manuscript.

REFERENCES

1. D.L. Leslie-Pelecky and R.D. Rieke, *Chem. Mater.*, **8**, 1770 (1996).
2. S. Shin and J. Jang, *Chem. Commun.*, **41**, 4230 (2007).
3. P.S. Antonel, G. Jorge, O.E. Perez, A. Butera, A.G. Leyva, and R.M. Negri, *J. Appl. Phys.*, **110**, 043920 (2011).
4. P. Chandrasekhar, *Conducting Polymers, Fundamentals and Applications: A Practical Approach*, Springer, New York (1999).
5. L. Lizarraga, E.M. Andrade, and F.V. Molina, *J. Electroanal. Chem.*, **561**, 127 (2004).
6. T.A. Skotheim and J. Reynolds, Eds., *Conjugated Polymers: Processing and Applications*, CRC Press, Boca Raton, FL, USA (2006).
7. P.S. Antonel, E. Völker, and F.V. Molina, *Polymer*, **53**, 2619 (2012).
8. A. Mirabedini, J. Foroughi, and G.G. Wallace, *RSC Adv.*, **6**, 44687 (2016).
9. K.K. Kanazawa, A.F. Diaz, R.H. Geiss, W.D. Gill, J.F. Kwak, J.A. Logan, J.F. Rabolt, and G.B. Street, *J. Chem. Soc. Chem. Commun.*, 854 (1979).
10. H. Ge and G.G. Wallace, *Polymer*, **33**, 2348 (1992).
11. T.V. Vernitskaya and O.N. Efimov, *Russian Chem. Rev.*, **66**, 443 (1997).
12. X. Yuan, X.-L. Ding, C.-Y. Wang, and Z.-F. Ma, *Energy Environ. Sci.*, **6**, 1105 (2013).
13. P. Camurlu, *RSC Adv.*, **4**, 55832 (2014).
14. Z.-B. Huang, G.-F. Yin, X.-M. Liao, and J.-W. Gu, *Front. Mater. Sci.*, **8**, 39 (2014).
15. P. Dallas, D. Niarchos, D. Vrbanic, N. Boukos, S. Pejovnik, C. Trapalis, and D. Petridis, *Polymer*, **48**, 2007 (2007).
16. S. Bose, T. Kuila, M.E. Uddin, N.H. Kim, A.K.T. Lau, and J.H. Lee, *Polymer*, **51**, 5921 (2010).
17. R.H. Kodama, *J. Magn. Magn. Mater.*, **200**, 359 (1999).
18. S.R. Chowdhury and E.K. Yanful, *J. Environ. Manage.*, **91**, 2238 (2010).
19. J.S. Beveridge, J.R. Stephens, and M.E. Williams, *Annu. Rev. Anal. Chem.*, **4**(**1**), 251 (2011).
20. J.L. Dormann, D. Fiorani, E. Tronc, "Magnetic relaxation in fine-particle systems," in *Advances in Chemical Physics*, vol. **98**, John Wiley & Sons, Inc., New York, 283 (2007).
21. J. Jin, K. Hashimoto, and S. Ohkoshi, *J. Mater. Chem.*, **15**, 1067 (2005).
22. A. Tavakoli, M. Sohrabi, and A. Kargari, *Chem. Pap.*, **61**, 151 (2007).
23. Y.I. Kim, D. Kim, and C.S. Lee, *Phys. B*, **337**, 42 (2003).
24. G. Mu, X. Pan, N. Chen, K. Gan, and M. Gu, *Mater. Res. Bull.*, **43**, 1369 (2008).
25. B. Leven and G. Dumpich, *Phys. Rev. B*, **71**, 064411 (2005).
26. H. Chen, D. Tang, B. Zhang, B. Liu, Y. Cui, and G. Chen, *Talanta*, **91**, 95 (2012).
27. E. Mazarío, P. Herrasti, M.P. Morales, and N. Menéndez, *Nanotechnology*, **23**, 355708 (2012).
28. Z. Guo, K. Shin, A.B. Karki, D.P. Young, R.B. Kaner, and H.T. Hahn, *J. Nanopart. Res.*, **11**, 1441 (2009).
29. C.S. Priya and G. Velraj, *Mater. Lett.*, **77**, 29 (2012).
30. D.E. Park, H.S. Chae, H.J. Choi, and A. Maity, *J. Mater. Chem. C*, **3**, 3150 (2015).
31. H. Wang, N. Ma, Z. Yan, L. Deng, J. He, Y. Hou, Y. Jiang, and G. Yu, *Nanoscale*, **7**, 7189 (2015).
32. K. Singh, A. Ohlan, P. Saini, and S.K. Dhawan, *Polym. Adv. Technol.*, **19**, 229 (2008).

33. I. Muñoz Resta, G. Horwitz, M. Lanús Mendez Elizalde, G. Jorge, F.V. Molina, and P.S. Antonel, *IEEE T. Magn.* (2013).
34. H. Gu, Y. Huang, X. Zhang, Q. Wang, J. Zhu, L. Shao, N. Haldolaarachchige, D.P. Young, S. Wei, and Z. Guo, *Polymer*, **53**, 801 (2012).
35. P.S. Antonel, F.M. Berhó, G. Jorge, and F.V. Molina, *Synth. Met.*, **199**, 292 (2015).
36. R. Gangopadhyay and A. De, *Chem. Mater.*, **12**, 608 (2000).
37. J. Pyun, *Polym. Rev.*, **47**, 231 (2007).
38. S. Radhakrishnan, S. Prakash, C.R.K. Rao, and M. Vijayan, *Electrochem. Solid State Lett.*, **12**, A84 (2009).
39. M. Bhaumik, T.Y. Leswifi, A. Maity, V.V. Srinivasu, and M.S. Onyango, *J. Hazard. Mater.*, **186**, 150 (2011).
40. S.C. Wuang, K.G. Neoh, E.-T. Kang, D.W. Pack, and D.E. Leckband, *J. Mater. Chem.*, **17**, 3354 (2007).
41. M. Qiao, X. Lei, Y. Ma, L. Tian, K. Su, and Q. Zhang, *Eng. Chem. Res.*, **55**, 6263 (2016).
42. R.-B. Yang, P.M. Reddy, C.-J. Chang, P.-A. Chen, J.-K. Chen, and C.-C. Chang, *Chem. Eng. J.*, **285**, 497 (2016).
43. Y. Qu, H. Yang, N. Yang, Y. Fan, H. Zhu, and G. Zhou, *Mater. Lett.*, **60**, 3548 (2006).
44. J.-M. Hu, G. Sheng, J.X. Zhang, C.W. Nan, and L.Q. Chen, *Appl. Phys. Lett.*, **98**, 112505–112505 (2011).
45. N.S. Gajbhiye, S. Prasad, and G. Blaji, *IEEE T. Magn.*, **35**, 2155 (1999).
46. S. Sun, H. Zeng, D.B. Robinson, S. Raoux, P.M. Rice, S.X. Wang, and G. Li, *J. Am. Chem. Soc.*, **126**, 273 (2004).
47. G.B. Street, T.C. Clarke, M. Krounbi, K. Kanazawa, V. Lee, P. Pfluger, J.C. Scott, and G. Weiser, *Mol. Cryst. Liquid Cryst.*, **83**, 253 (1982).
48. H. Kato, O. Nishikawa, T. Matsui, S. Honma, and H. Kokado, *J. Phys. Chem.*, **95**, 6014 (1991).
49. J. Lei, W. Liang, and C.R. Martin, *Synth. Met.*, **48**, 301 (1992).
50. R. Kostić, D. Raković, S.A. Stepanyan, I.E. Davidova, and L.A. Gribov, *J. Chem. Phys.*, **102**, 3104 (1995).
51. I. Rodríguez, B.R. Scharifker, and J. Mostany, *J. Electroanal. Chem.*, **491**, 117 (2000).
52. M. Khairy, *Synth. Met.*, **189**, 34 (2014).
53. G.D. Prasanna, H.S. Jayanna, A.R. Lamani, and S. Dash, *Synth. Met.*, **161**, 2306 (2011).
54. S. Mørup, M.F. Hansen, and C. Frandsen, *Beilstein J. Nanotechnol.*, **1**, 182 (2010).
55. K.H. Wu, Y.M. Shin, C.C. Yang, W.D. Ho, and J.S. Hsu, *J. Polym. Sci. A Polym. Chem.*, **44**, 2657 (2006).
56. P. Montoya, F. Jaramillo, J. Calderón, S.I. Córdoba de Torresi, and R.M. Torresi, *Electrochim. Acta*, **55**, 6116 (2010).
57. X. Zhang, X. Xu, T. Li, M. Lin, X. Lin, H. Zhang, H. Sun, and B. Yang, *ACS Appl. Mater. Interfaces*, **6**, 14552 (2014).
58. F. Bødker, S. Mørup, and S. Linderoth, *Phys. Rev. Lett.*, **72**, 282 (1994).
59. L. Néel, *J. Phys. Radium*, **15**, 225 (1954).
60. C.R. Vestal and Z.J. Zhang, *Nano Lett.*, **3**, 1739 (2003).
61. R.C. O'Handley, *Modern Magnetic Materials: Principles and Applications*, Wiley-Interscience, New York (1999).
62. Y. Long, Z. Chen, J. Shen, Z. Zhang, L. Zhang, K. Huang, M. Wan, A. Jin, C. Gu, and J.L. Duvail, *Nanotechnology*, **17**, 5903 (2006).
63. M. Romero, R. Faccio, H. Pardo, M.A. Tumelero, B. Montenegro, C. Campos Plá Cid, A.A. Pasa, and Á.W. Mombrú, *J. Mater. Chem. C*, **3**, 12040 (2015).